Extreme events in computational turbulence

P. K. Yeung[a], X. M. Zhai[b], and Katepalli R. Sreenivasan[c,1]

[a]Schools of Aerospace Engineering and Mechanical Engineering, Georgia Institute of Technology, Atlanta, GA 30332; [b]School of Aerospace Engineering, Georgia Institute of Technology, Atlanta, GA 30332; and [c]Department of Physics, Department of Mechanical and Aerospace Engineering and Courant Institute of Mathematical Sciences, New York University, New York, NY 10012

Contributed by Katepalli R. Sreenivasan, September 4, 2015 (sent for review July 14, 2015; reviewed by Celso Grebogi, Raymond Shaw, and Harry L. Swinney)

We have performed direct numerical simulations of homogeneous and isotropic turbulence in a periodic box with 8,192^3 grid points. These are the largest simulations performed, to date, aimed at improving our understanding of turbulence small-scale structure. We present some basic statistical results and focus on "extreme" events (whose magnitudes are several tens of thousands the mean value). The structure of these extreme events is quite different from that of moderately large events (of the order of 10 times the mean value). In particular, intense vorticity occurs primarily in the form of tubes for moderately large events whereas it is much more "chunky" for extreme events (though probably overlaid on the traditional vortex tubes). We track the temporal evolution of extreme events and find that they are generally short-lived. Extreme magnitudes of energy dissipation rate and enstrophy occur simultaneously in space and remain nearly colocated during their evolution.

turbulence | intermittency | extreme events | petascale computing | fluid dynamics

Fluid motions encountered in most circumstances are typically turbulent; therefore a good understanding of the subject is essential both for intrinsic scientific reasons and for advancing important technologies, e.g., improving jet engine performance. The difficulty of the subject (1, 2) has unfortunately consigned our present understanding to be partial at best. A milestone of turbulence theory consists of the similarity hypotheses of Kolmogorov (3, 4) and their various descendant scaling theories. In refs. 5 and 6, one can find a fair summary of the theoretical ideas as well as the considerable experimental work devoted to assessing their veracity. Rapid advances in computing power in recent decades have made computations increasingly important in advancing our understanding of the subject. Key quantities that cannot yet be measured in experiments can instead be computed by the so-called direct numerical simulation (DNS; e.g., see ref. 7), in which the exact equations of motion based on mass and momentum conservation are integrated numerically in time and space. The DNS data are capable of providing a wealth of quantitative detail (see, e.g., ref. 8) and improved qualitative understanding. In this paper, we present results from the largest DNS, to date, of isotropic turbulence aimed at the small-scale structure, rendered statistically stationary by large-scale forcing. We focus on the extreme events (to be made more precise momentarily).

Turbulent flows consist of disorderly fluctuations in all measurable properties over a range of scales in both space and time. These fluctuations produce a combination of changes in shape and orientation of an infinitesimal fluid element and can affect quantities of practical interest, such as the tendency of tiny water vapor droplets to collide and grow to millimeter-size rain drops in atmospheric clouds (9). One of the key fluctuating quantities is the energy dissipation rate, $\epsilon = 2\nu s_{ij}s_{ij}$, where ν is the kinematic viscosity, s_{ij} is the rate of strain given by $\frac{1}{2}(\partial u_i/\partial x_j + \partial u_j/\partial x_i)$, u_i being the velocity in the direction i, and we have used Einstein's summation convention. The second key quantity is the turbulent vorticity, $\vec{\omega} = \nabla \times \vec{u}$. From $\vec{\omega}$, one can define the instantaneous enstrophy $\Omega = \omega_i\omega_i$, whose mean value multiplied by the kinematic viscosity is equal to the mean dissipation rate, although their interrelationship is more complex locally. Here, we focus on ε and Ω. The mean energy dissipation rate is equal to the rate of energy transfer from large scales of turbulence to small scales, and is thus a key quantity that characterizes the nonlinear interaction among the various scales excited in a turbulent flow. An extremely high dissipation rate (which implies high strain rate) can, for example, tear apart a flame surface and lead to local extinction in reacting systems (10). Fluctuations of enstrophy are likewise crucial in attempts to describe the structure of turbulence as (primarily) a collection of vortices of various intensities, sizes, and spacing (11).

Our focus on small-scale properties ϵ and Ω suggests that it is adequate to consider homogeneous and isotropic turbulence, which is what we do here. The simulations are performed using well-established Fourier pseudospectral methods on 3D periodic domains (8). Advances in computing have allowed simulations to increase in size from 512^3 grid points in the 1990s to 4,096^3 in 2003 (12). The present simulations on an 8,192^3 box (see *Simulation and Data Processing Methodology*) push toward attaining higher Reynolds numbers. See the legend for Table 1 for specific definitions of the Reynolds number; it suffices here to say that it determines the range of excited scales. This quest to increase the Reynolds number and the need to better resolve the small scales is the crux of DNS methods today (13, 14). As the flow Reynolds number increases (which is the main reason for increasing the size of the simulations), ϵ and Ω fluctuate more and more wildly in space and time. This property of intermittency is thought to be a central trait of turbulence, and indeed of all strongly nonlinear systems. For the Reynolds numbers attained in the present simulations, ϵ and Ω display fluctuations of the order up to 10^5 times their mean values. These extreme events are very fast-changing and require frequent sampling. We capture them faithfully and study them here: We not only study several standard statistical characteristics

Significance

In the last decade or so, massive computations of turbulence performed by solving the exact equations of hydrodynamic turbulence have provided new quantitative data and enhanced our understanding. This paper presents results from the largest such computations, to date, devoted to the study of small scales. We focus on "extreme events" in energy dissipation and squared vorticity (enstrophy). For the Reynolds numbers of these simulations, events as large as 10^5 times the mean value are observed, albeit rarely. The structure of these extreme events is quite different from that believed previously. The major theme of this and related work is that huge fluctuations exist in hydrodynamic turbulence and that they have basic consequences to turbulence (as is the case in other nonlinear fields).

Author contributions: P.K.Y. and K.R.S. designed research; P.K.Y. and X.M.Z. performed research; P.K.Y. and X.M.Z. analyzed data; and P.K.Y. and K.R.S. wrote the paper.

Reviewers: C.G., University of Aberdeen; R.S., Michigan Technological University; and H.L.S., University of Texas at Austin.

The authors declare no conflict of interest.

Freely available online through the PNAS open access option.

[1]To whom correspondence should be addressed. Email: krs3@nyu.edu.

This article contains supporting information online at www.pnas.org/lookup/suppl/doi:10.1073/pnas.1517368112/-/DCSupplemental.

as well as their spatial and temporal nature but also discuss questions of their spatial simultaneity and geometric shape. We show that they are quite different in character from those that have been routinely designated as extreme events until now. We proceed below by elaborating on the concept of extreme events and the challenges they pose. Questions of accuracy, including effects of numerical resolution, statistical convergence, and machine precision, are addressed briefly in *Supporting Information*.

Extreme Events in Small Scales

In the turbulence literature (e.g., ref. 15), the phrase "extreme events" has referred to fluctuations that are a few times [typically $O(10)$] the mean or standard deviation. This characterization is not unreasonable at low Reynolds numbers where events of much higher amplitudes are not common. However, the situation at high Reynolds numbers, as appropriate to the present simulations, is quite different: In Fig. 1, which shows the normalized probability density functions (PDFs) of dissipation and enstrophy, events with strengths of the order of tens of thousands of the mean value occur, albeit rarely. This suggests that the use of the word "extreme" must be reserved for events that are thousands (or more) of mean values in strength, and that we should use the designation "moderately large" for those previously regarded as extreme. The truly extreme events are often not well-captured (or captured with smoothing), partly because of inadequate resolution and partly because they do not occur at very low Reynolds numbers. Experiments likewise do not resolve such high-intensity events. It is thus no surprise that in many experiments and simulations (e.g., refs. 16–18), dissipation or enstrophy of this level has not been reported. However, the present data confirm recent results (14, 19), which displayed, even at a lower (but still high) Reynolds number, samples of dissipation and enstrophy that are many thousands of mean values. It should thus come as no surprise if the structure of the extreme events should turn out to be quite different from that of moderately large events. In particular, vorticity occurs primarily in the form of tubes in the moderately large events, whereas the extreme events are not of that form, as we shall show; further, for extreme events, energy dissipation rate and enstrophy occur essentially simultaneously in space.

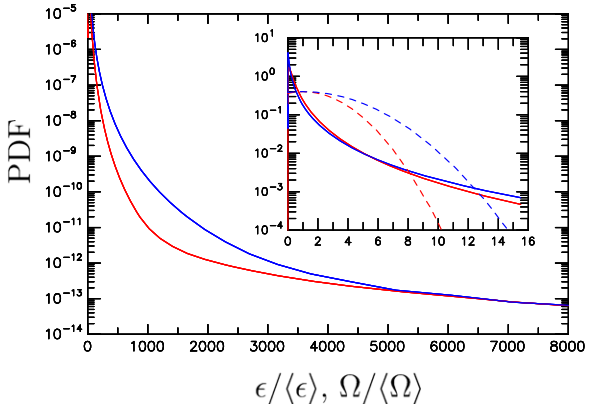

Fig. 1. Ensemble-averaged PDFs of normalized dissipation (red) and enstrophy (blue) from $8{,}192^3$ simulation at $R_\lambda \approx 1{,}300$, with $k_{max}\eta \approx 2$. *Inset* shows data for 0–16 mean values. Dashed curves in *Inset* show positive halves of Gaussian distributions with equal variances; they serve only a pedantic purpose because dissipation and enstrophy are both positive definite. Rare events occur enormously more frequently than can be anticipated by Gaussian distributions—by some 10 orders of magnitude when the abscissae values reach 50 or smaller, and by some 250 orders of magnitude for abscissae values of 1,000. Although the data shown are averaged over 14 instantaneous snapshots, the main features are robust: Every snapshot possesses similar features.

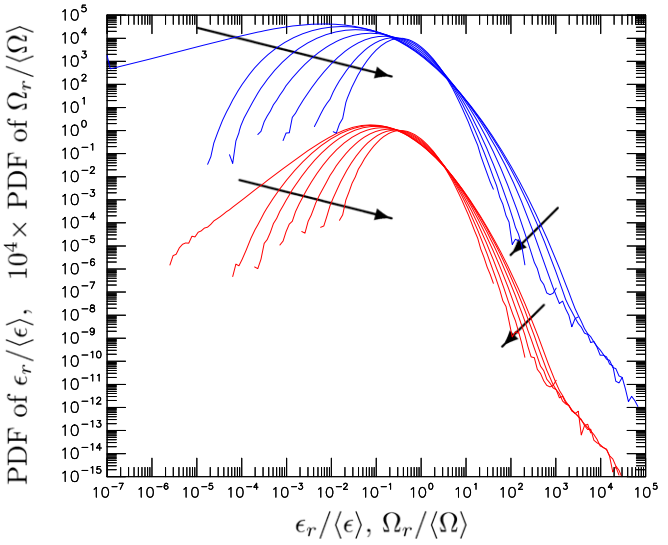

Fig. 2. PDFs of $\epsilon_r/\langle\epsilon\rangle$ (red) and $\Omega_r/\langle\Omega\rangle$ (blue) for r corresponding to subcubes with linear dimensions of 1, 2, 4, 8, 16, 32, and 64 grid points in each direction (increasing in the direction of the arrows). For clarity, the PDFs of $\Omega_r/\langle\Omega\rangle$ are offset upward by 10^4.

One further observation on Fig. 1 is useful. It can be seen that events of moderate intensity (of order tens to hundreds of the mean) are more likely for the enstrophy than dissipation. At high Reynolds numbers as here, the PDFs of dissipation and enstrophy tend to converge toward higher values of both variables. This result has an important consequence: It suggests that higher moments of ϵ and Ω would be nearly identical (because they would depend on the tails), as has been suggested on the basis of theoretical arguments (20, 21). Low Reynolds number PDFs, which essentially truncate considerably to the left of where the tails of the two PDFs collapse, do not show congruity with theory.

Simulation and Data Processing Methodology

The considerations above point to a need for advanced computing that pushes the envelope of current limits. DNS of turbulence using tens or even hundreds of billions of grid points is a demanding task that requires petascale resources in processing speed and data management. Key features of our parallel algorithms include a 2D domain decomposition*, exploiting truncation (for dealiasing) in wavenumber space to reduce communication and computational needs, remote memory addressing for interprocessor communication, and multithreading for multicored on-node parallelism. Although pseudospectral codes tend to be communication-intensive, they perform significantly better if a favorable network topology is available. Accordingly, our code has scaled reasonably well up to $2^{18} = 262{,}144$ cores on Blue Waters, a Cray XE/XK machine rated at more than 10 petaflops in aggregate speed located at the University of Illinois, Urbana–Champaign.

In the present $8{,}192^3$ simulation, we have achieved stationary state by forcing the energy spectrum in the lowest wavenumber shells, as in our earlier $4{,}096^3$ simulations (19), and the Reynolds number is increased by reducing the viscosity. The Taylor-scale Reynolds number reached is 1,300. It is only slightly higher than in earlier $4{,}096^3$ simulations by others and by us, because our grid spacing of 1.5 Kolmogorov length scales is significantly better than that used earlier in such large simulations. With a dedicated 0.5-petabyte storage capacity, we were able to save

*Donzis DA, Yeung PK, Pekurovsky D, 2008 TeraGrid Conference, June 9–13, 2008, Las Vegas, NV.

Table 1. Parameters of the $8{,}192^3$ simulation performed in this paper

Parameter	Value
Kinematic viscosity (ν)	0.00004385
Longitudinal length scale (L_1)	1.246
Taylor microscale (λ)	0.036
Kolmogorov length scale (η)	0.000504
Kolmogorov time scale (τ_η)	0.005794
Root-mean-squared velocity (u')	1.583
Mean dissipation rate ($\langle\epsilon\rangle$)	1.306

Parameters include length scales of interest, the intensity of velocity fluctuations, and the mean rate of energy dissipation. The integral length scale L_1, which represents the size of the large eddies (where most of the energy resides), is about 1/5 of the domain size (L_0, which is set to 2π units). The so-called large-eddy Reynolds number, $u'L_1/\nu$ is ∼45,000. The intermediate length scale, the so-called Taylor microscale ($\lambda = u'\Big/\sqrt{\langle(\partial u/\partial x)^2\rangle}$), is used to define the Reynolds number $R_\lambda = u'\lambda/\nu$, which is about 1,300 for these simulations. The normalized average energy dissipation rate $\langle\epsilon\rangle L_1/u'^3 = 0.410$ is consistent with known results on dissipative anomaly (37), which states that although most of the dissipation occurs at viscosity-affected small scales, the average rate of dissipation is determined by the large-scale parameters. The Kolmogorov length scale, $\eta = (\nu^3/\langle\epsilon\rangle)^{1/4}$, characteristic of the dissipative scales, is about 1.5 times the grid spacing $\Delta x = 2\pi/N$, where $N = 8{,}192$. The Kolmogorov time scale is $\tau_\eta = (\nu/\langle\epsilon\rangle)^{1/2}$. The numbers in this table have been averaged over a time span of about 2.5 large-eddy time scales (L_1/u'). The actual units of these quantities can be expressed in any self-consistent system.

many instantaneous snapshots of the Fourier velocity fields, from which many one- and two-point statistics can be computed and subsequently ensemble-averaged. Statistics such as the PDFs of dissipation rate and enstrophy can also be obtained "on the fly" within the DNS code itself. Qualitative information on spatial structure is obtained by 3D visualization, with focus on local regions of intense activity.

Table 1 lists some parameters of interest. They include information on length scales, turbulence intensity, and the scaling of the averaged dissipation rate. The nondimensional quantities behave in a manner expected of high Reynolds number turbulence based on past publications by us and by other groups in the field (8, 19).

Spatial Structure

To understand the spatial structure of extreme events, we identify them in the DNS database and zoom in on their neighborhoods. In using a 2D domain decomposition, the 3D solution domain is divided into a number of "pencils," which are elongated subdomains with two short (not necessarily equal) dimensions and one full-length dimension. Three-dimensional subvolumes, or "subcubes" can be formed by further subdividing each pencil along its longest direction. Larger subcubes not completely residing within a single pencil can be formed by merging neighboring pencils. The net result is a 3D domain decomposition achieved in an efficient manner. In addition to facilitating visualization, this approach allows us to compute the statistics of local averages of dissipation and enstrophy (over a subcube of linear size r, say), these being the key element of Kolmogorov's (4) refined similarity theory. Local averaging smooths out extremely large values of ϵ_r and Ω_r increasingly as r increases; extremely small values also become less extreme. Fig. 2 shows the PDFs of both $\epsilon_r/\langle\epsilon\rangle$ and $\Omega_r/\langle\Omega\rangle$ for a set of logarithmically spaced values of r. The outermost line corresponding to the highest resolution has a power-law tail on the left, which has been shown (19) to arise from the fact that small strain rates and vorticity components are associated with the Gaussian core for the PDF of velocity gradient fluctuations. As r increases, the ranges of values, or variability, of both ϵ_r and Ω_r decrease. For $\epsilon_r/\langle\epsilon\rangle$ (likewise for $\Omega_r/\langle\Omega\rangle$) exceeding 10^3, the curves for the smallest few values of r resemble a power-law tail, which is ultimately truncated (so that the moments do exist). This power-law tail is observed only for the smallest few sizes of the subcube, corresponding to an activity that is localized in space.

The intricate detail often present in turbulence datasets makes 3D scientific visualization a useful investigative tool. Given our purpose, it is not necessary to visualize the prohibitively large full-field $8{,}192^3$ snapshots, but it is important to focus on local regions where extreme events reside and pick the subcubes that are large enough. We mainly use 3D color surfaces but note that the appearance of the resulting images can depend strongly on the contour threshold chosen.

Fig. 3 shows a collection of nine images, some showing magnified views of a smaller subcube to emphasize important features. In Fig. 3*A*, we begin with a low threshold of 10, and a subcube of 768^3. Although the spotty nature of ϵ and Ω exceeding this threshold is apparent, this image does not reveal much about extreme events because the threshold is chosen low. Fig. 3 *B* and *C* shows the effect of increasing the threshold to 30 (Fig. 3*B*) and 100 (Fig. 3*C*), while zooming in on a more compact (256^3) subcube. As expected, the volume enclosed by contour surfaces shrinks substantially as the threshold is raised. At the threshold of 100, filament-like structures are quite visible in enstrophy. The fraction of space in cyan also becomes significantly higher than that in red, which is consistent with the contrast between probability of occurrence of ϵ and Ω around this threshold (see Fig. 1).

Continuing, Fig. 3 *D–F* shows the contrasts between images where ϵ and Ω are rendered separately as well as simultaneously. At the threshold of 300, both dissipation and enstrophy show chunky structures that are only modestly elongated, but enstrophy is slightly more space-filling. This main structure is distinct from a thinner vortex filament seen near the upper right corner of Fig. 3*E*. In Fig. 3*F*, where both variables are shown, the chunky region appears as mainly red, which implies that the dissipation contour surface subsumes the region of peak enstrophy. This observation is consistent with the notion that high-vorticity regions at this level of intensity tend to be wrapped around by sheets of intense dissipation (and thus the strain rate) (22).

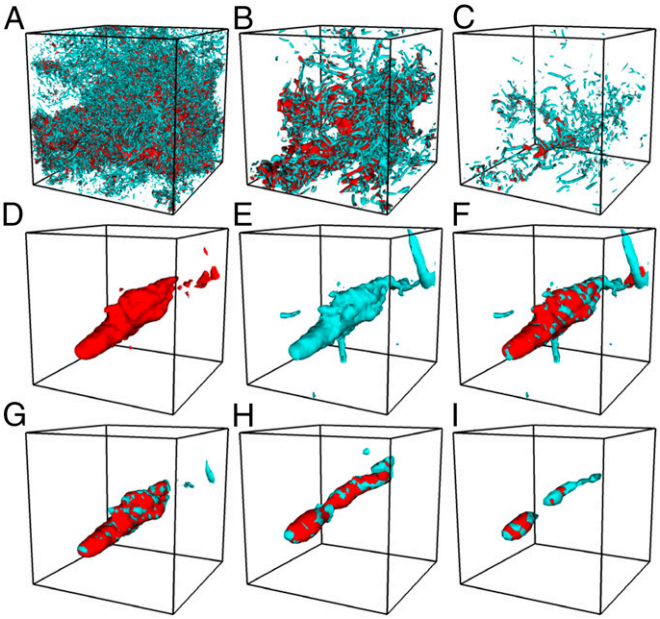

Fig. 3. Perspective views of 3D contour surfaces of dissipation (red) and enstrophy (cyan) extracted from a randomly chosen (but representative) $8{,}192^3$ instantaneous snapshot, at different thresholds (in multiples of mean values) and for different sized subcubes: (*A*) 10, 768^3; (*B*) 30, 256^3; (*C*) 100, 256^3; (*D–F*): 300, 51^3; (*G*) 600, 51^3; (*H*) 4,800, 31^3; and (*I*) 9,600, 31^3. Both dissipation and enstrophy are shown in all frames but *D* and *E*.

PHYSICS

Finally, Fig. 3 *G–I* are images obtained at yet higher thresholds. A comparison between Fig. 3 *F* and *G* shows that some vortex filaments visible at threshold 300 are no longer present at threshold 600, while the main structure with a chunky appearance remains largely intact. In Fig. 3*H* as the threshold is raised further to 4,800, the structure becomes somewhat slimmer although not as slender as typical worm-like vortex filament of refs. 12 and 23. In Fig. 3*I* for the threshold of 9,600, the structure seems to break into two—one of which looks like a blob and and the other like a filament. The wrapping around of vortex filaments by sheet-like dissipation is now less pronounced, as the red color itself is now covering the chunky main structure less completely. Closer examination (e.g., by raising the threshold even higher) indicates that the global maximum is located inside the blob-like region in the lower half of Fig. 3*I*.

To ascertain that the snapshot used to produce Fig. 3 is representative, and to illustrate the effect of the Reynolds number, in Fig. 4, we show dissipation and enstrophy contour surfaces from three $8{,}192^3$ snapshots, and one $2{,}048^3$ at a lower Reynolds number. Fig. 4*A* is the same as Fig. 3*F* but repeated here for convenience. Fig. 4*A–C* shows a dominant chunky structure with some worm-like vortex filaments nearby. All three images are consistent with the scenario of sheets of intense dissipation being wrapped around a region of intense enstrophy. The chunky structure itself contains the grid location where both dissipation and enstrophy attain their maximum values. The near colocation of dissipation and enstrophy is apparently a very robust feature—in all of the $8{,}192^3$ snapshots that we examined, the maxima of dissipation and enstrophy are located just one or two grid points apart. However, Fig. 4*D*, for a lower Reynolds number, is characteristically different: The dominant structure there appears to be vortex filaments that are only partially surrounded by intense dissipation. Peak dissipation and peak enstrophy in the lower Reynolds number data are also not colocated.

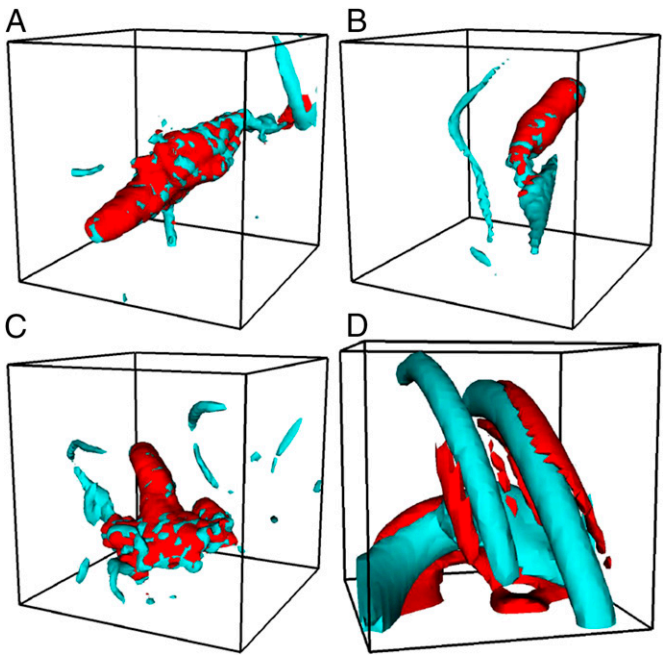

Fig. 4. Color contours based on (*A–C*) three instantaneous snapshots from the $8{,}192^3$ simulation at $R_\lambda \approx 1{,}300$, contrasted with data from (*D*) $2{,}048^3$ simulation at $R_\lambda \approx 400$. The contour thresholds used were 300 for data at $R_\lambda \approx 1{,}300$ and 70 for data at $R_\lambda \approx 400$. The subcubes are 51^3 in extent in *A–C* and 31^3 in *D*.

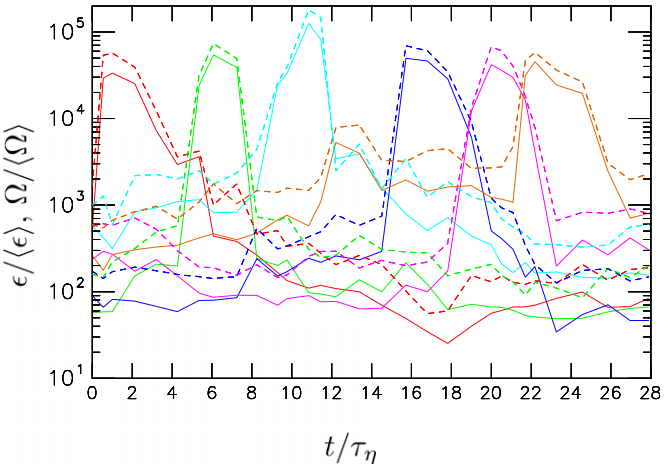

Fig. 5. Sample time traces of extreme events in normalized dissipation (solid lines) and enstrophy (dashed lines), over a time period of 28 Kolmogorov time scales (τ_η) in the $8{,}192^3$ simulation with double-precision arithmetic. Each color represents one selected event. Data points are plotted at times approximately one τ_η apart.

Temporal Evolution

Because small-scale motions are traditionally thought to be associated with short time scales, extreme events in dissipation and enstrophy may be expected to have short lifetimes. On the other hand, strong and organized vortex structures have long been known to be relatively persistent, visually identifiable, and coherent over a significant fraction of a large-eddy timescale (24, 25). We are thus interested in characterizing the temporal evolution (and sustenance) of the extreme events studied here, including the physical mechanism(s) that cause these extreme events to form (as addressed in a different context in ref. 15).

To obtain some concrete data, we examine a number of instantaneous velocity fields that have been saved at relatively close time intervals over a significant duration. For each instantaneous snapshot, we divide the solution domain into a number of subcubes of fixed size (of 256^3 in the case of $8{,}192^3$ datasets). By identifying the maxima of dissipation and enstrophy within each subcube and then repeating the procedure for all subcubes, we obtain their global maximum values for a given snapshot, and also identify the subcubes in which those maximum values reside. Only if a subcube contains the global maximum in two successive snapshots is it considered to contain the extreme event (merely for purposes of robustness). We examine the time history of the local maxima in such subcubes over the available time period, which is many times longer than the typical time scale of the extreme events.

We use data from a double-precision segment of the simulations in which 31 snapshots of velocity fields were saved over a period of about 28 Kolmogorov time scales. The maxima of $\epsilon/\langle\epsilon\rangle$ and $\Omega/\langle\Omega\rangle$ over all space in these snapshots ranged from 1.9×10^4 to 1.3×10^5 and 2.6×10^4 to 1.8×10^5, respectively. Fig. 5 shows the time traces of several extreme events (limited to six to avoid excessive clutter), identified using the criteria described above. It is clear that all of the chosen events undergo periods of growth, sustenance, and eventual decay. (The fact that all of the events appear to have nearly the same peak amplitudes is related to the logarithmic scale of the amplitude.) Events of extreme dissipation and extreme enstrophy follow each other very closely, consistent with the near colocation of peak dissipation and enstrophy in single-time snapshots noted earlier. As a measure of their lifetime, each event is seen to exceed 1,000 in magnitude for about three to five Kolmogorov time scales, whereas all time

traces shown retain amplitudes above 50 almost throughout the entire 28 τ_η time period shown. At the Reynolds number of these data, the large-eddy turnover time is roughly 120 τ_η. These observations are thus consistent with the conventional notion of intense vorticity structures being relatively persistent in time—except that extreme events retain their "extreme" character only for a few τ_η.

In principle, extreme dissipation or enstrophy at a point can be the result of a strong production mechanism that is localized in space and time, and/or a short-term accumulation due to turbulent transport. On the other hand, effects that tend to act against or limit extreme values include viscous diffusion (a transport effect that tends to reduce any localized spatial inhomogeneities) and viscous dissipation, which destroys the velocity gradient fluctuations that underlie both dissipation and enstrophy. To assess the relative importance of these distinct effects for intense-to-extreme enstrophy, we can compute all of the terms in the instantaneous enstrophy budget equation,

$$\frac{\partial \Omega}{\partial t} = -\frac{\partial u_j \Omega}{\partial x_j} + \nu \frac{\partial^2 \Omega}{\partial x_j \partial x_j} + 2\omega_i \omega_j s_{ij} - 2\nu \frac{\partial \omega_i}{\partial x_j} \frac{\partial \omega_i}{\partial x_j}, \qquad [1]$$

which expresses the effects of transport due to velocity fluctuations, transport due to molecular viscosity, production via vortex stretching (due to conservation of angular momentum), and dissipation due to viscous effects. In our simulations, because of statistical stationarity in time and statistical homogeneity in space, application of averaging to Eq. **1** gives

$$\langle \omega_i \omega_j s_{ij} \rangle = \nu \left\langle \frac{\partial \omega_i}{\partial x_j} \frac{\partial \omega_i}{\partial x_j} \right\rangle, \qquad [2]$$

which is exactly true for homogeneous and isotropic turbulence and approximately true for all flows at sufficiently high Reynolds numbers (26). However, all terms are (potentially) important if conditioned on different ranges of the normalized dissipation and/or enstrophy.

Fig. 6 shows the conditional averages for each term in Eq. **1**, for two distinct ranges of the normalized enstrophy. Production is the dominant positive contribution, increasing strongly with the enstrophy. Although this result is not unexpected, we caution that the value of the term $\omega_i \omega_j s_{ij}$ depends on the alignment between the vorticity vector and the principal axes of the strain rate fluctuations (27). The turbulent transport term appears to be trivially small for almost all values of enstrophy. Both viscous diffusion and viscous dissipation have negative contributions, whose magnitudes are similar at both low and moderately high enstrophy. For very high and extreme enstrophy, viscous diffusion is the strongest, although viscous dissipation remains significant as well. These results imply that viscous diffusion is the main process that prevents infinitely high enstrophy.

Conclusions and Implications

One of the highlights of turbulence theory is Kolmogorov's pioneering work (3), which predicts a $-5/3$ power of the energy spectrum in the so-called inertial range (the intermediate range of scales which are neither energy-containing nor dissipative). At least at a superficial level (and with some plausible corrections), this prediction is supported by experiments and simulations. This apparent success has solidified the notion of similarity underlying Kolmogorov's theory. An unspoken belief has been that the only change produced by increasing the Reynolds number is to extend the inertial range with no other structural changes: For example, the turbulent eddies retain their shape, as often shown in schematic diagrams that depict spherical eddies as remaining spherical with ever decreasing sizes, the smallest being at the Kolmogorov scale

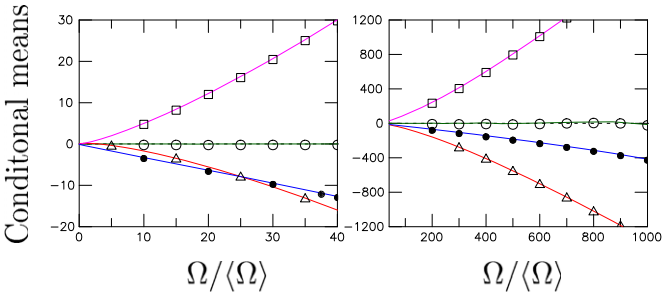

Fig. 6. Conditional mean values of turbulent transport (○), viscous diffusion (△), nonlinear production (□), and viscous dissipation (●) in the enstrophy evolution equation, given the instantaneous normalized enstrophy, and all normalized by τ_η^3. *Left* and *Right* show data for $0 \le \Omega/\langle\Omega\rangle \le 40$ and $40 \le \Omega/\langle\Omega\rangle \le 1{,}000$, respectively. Trends for $\Omega/\langle\Omega\rangle > 1{,}000$ are similar.

(see, e.g., ref. 5). The next major improvement in our understanding occurred when it was realized that more complex changes accompany the increase in Reynolds number. For example, the smaller scales (at least those with moderately high intensities) are elongated vortices; that is, the similarity is not self-similar but self-affine (28). This has been confirmed for moderately strong events by several investigators, most convincingly by Ishihara et al. (29).

The present simulations at the highest Reynolds numbers to date—with the small scales well resolved—suggest something even more complex: With increasing Reynolds numbers, the extreme events assume a form that is not characteristic of similar events at low Reynolds numbers. Our results show that, for the Reynolds numbers of these simulations, events as large as 10^5 times the mean value obtain, albeit rarely. They appear chunky in character, unlike elongated vortex tubes. We track the temporal evolution of these extreme events and find that they are generally short-lived. Extreme magnitudes of energy dissipation rate and enstrophy occur essentially simultaneously in space and remain nearly colocated during their evolution. This is the insight of the present work. The fact that extreme events do not preserve the same form at different Reynolds numbers strongly underlines that the large amplitude events (more broadly, the phenomenon of intermittency) at one Reynolds number cannot be understood by some simple transformation of those at another (lower) Reynolds number. This may well be the source of anomaly that turbulence is known to possess (e.g., ref. 6). We do not yet know how this insight is related to the source of anomaly so beautifully explored quantitatively for the Kraichnan model (30) of passive scalar turbulence (e.g., refs. 31–33).

Extreme events at the level of intensity reported in this paper are expected to have a strong influence, for instance, on the Lagrangian intermittency for infinitesimal fluid particles (34), and the local structure of the acceleration field in the neighborhood of events of extreme dissipation and/or extreme enstrophy (35).

A brief speculation is worthwhile: What might one see in well-resolved simulations at even higher Reynolds numbers? Will new types of extreme events (or singular structures) emerge? The current understanding is that, in the singularity, exponents saturate in the limit of infinite Reynolds number (see ref. 36). One does not know if that asymptotic state has been reached in these simulations.

ACKNOWLEDGMENTS. The authors gratefully acknowledge dedicated assistance from consultants and staff on the Blue Waters Project, which is supported by National Science Foundation (NSF) at the National Center for Supercomputing Applications, University of Illinois at Urbana–Champaign. This work is supported by NSF Grant ACI-1036170 under the Petascale Resource Allocations program.

1. Lumley JL, Yaglom AM (2001) A century of turbulence. *Flow. Turbul Combust* 66(3):241–286.
2. Sreenivasan KR (1999) Fluid turbulence. *Rev Mod Phys* 71(2):s383–s395.
3. Kolmogorov AN (1941) The local structure of turbulence in an incompressible viscous fluid with very large Reynolds numbers. *Dokl Akad Nauk SSSR* 30:301–305.
4. Kolmogorov AN (1962) A refinement of previous hypotheses concerning the local structure of a viscous incompressible fluid. *J Fluid Mech* 13:82–85.
5. Frisch U (1995) *Turbulence: The Legacy of A. N. Kolmogorov* (Cambridge Univ Press, Cambridge, UK).
6. Sreenivasan KR, Antonia RA (1997) The phenomenology of small-scale turbulence. *Annu Rev Fluid Mech* 29:435–472.
7. Moin P, Mahesh K (1998) Direct numerical simulation: A tool in turbulence research. *Annu Rev Fluid Mech* 30:539–578.
8. Ishihara T, Gotoh T, Kaneda Y (2009) Study of high-Reynolds number isotropic turbulence by direct numerical simulation. *Annu Rev Fluid Mech* 41:165–180.
9. Shaw RA (2003) Particle-turbulence interactions in atmospheric clouds. *Annu Rev Fluid Mech* 28:183–227.
10. Pitsch H, Steiner H (2000) Scalar mixing and dissipation rate in large-eddy simulations of non-premixed turbulent combustion. *Proc Combust Inst* 28(1):41–49.
11. Jimenez J, Wray AA, Saffman PG, Rogallo RS (1993) The structure of intense vorticity in isotropic turbulence. *J Fluid Mech* 255:65–90.
12. Kaneda Y, Ishihara T, Yokokawa M, Itakura K, Uno A (2003) Energy dissipation rate and energy spectrum in high resolution direct numerical simulations of turbulence in a periodic box. *Phys Fluids* 15(2):L21–L24.
13. Yakhot V, Sreenivasan KR (2005) Anomalous scaling of structure functions and dynamic constraints on turbulence simulations. *J Stat Phys* 121(5-6):823–841.
14. Donzis DA, Yeung PK, Sreenivasan KR (2008) Dissipation and enstrophy in isotropic turbulence: Scaling and resolution effects in direct numerical simulations. *Phys Fluids* 20(4):045108.
15. Donzis DA, Sreenivasan KR (2010) Short-term forecasts and scaling of intense events in turbulence. *J Fluid Mech* 647:13–26.
16. Bershadskii A, Kit E, Tsinober A (1994) Strongly localized events of energy, dissipation, enstrophy and enstrophy generation in turbulent flows. *Fluid Dyn Res* 14(2):71–101.
17. Chen S, Sreenivasan KR, Nelkin M (1997) Inertial range scalings of dissipation and enstrophy in isotropic turbulence. *Phys Rev Lett* 79(7):1253.
18. Zeff BW, et al. (2003) Measuring intense rotation and dissipation in turbulent flows. *Nature* 421(6919):146–149.
19. Yeung PK, Donzis DA, Sreenivasan KR (2012) Dissipation, enstrophy and pressure statistics in turbulence simulations at high Reynolds numbers. *J Fluid Mech* 700:5–15.
20. Lvov VS, Procaccia I (1996) The universal scaling exponents of anisotropy in turbulence and their measurement. *Phys Fluids* 8(10):2565–2567.
21. Nelkin M (1999) Enstrophy and dissipation must have the same scaling exponents in the high Reynolds number limit of fluid turbulence. *Phys Fluids* 11(8):2202–2204.
22. Karahawa G (2005) Energy dissipation in spiral vortex layers wrapped around a straight vortex tube. *Phys Fluids* 17(5):055111.
23. Jimenez J (2003) Computing high-Reynolds-number turbulence: Will simulations ever replace experiments? *J Turbul* 4(22):22.
24. Cantwell BJ (1981) Organized motion in turbulent flow. *Annu Rev Fluid Mech* 13: 457–515.
25. Jeong J, Hussain F (1995) On the identification of a vortex. *J Fluid Mech* 285:69–94.
26. Tennekes H, Lumley JL (1972) *A First Course in Turbulence* (MIT Press, Cambridge, MA).
27. Ashurst WT, Kerstein AR, Kerr RM, Gibson CH (1987) Alignment of vorticity and scalar gradient with strain rate in simulated Navier-Stokes turbulence. *Phys Fluids* 30(8): 2343–2353.
28. Mandelbrot BB (1983) *The Fractal Geometry of Nature* (Freeman, New York).
29. Ishihara T, Kaneda Y, Yokokawa M, Itakura K, Uno A (2007) Small-scale statistics in high resolution direct numerical simulation of turbulence: Reynolds number dependence of one-point velocity gradient statistics. *J Fluid Mech* 592:335–366.
30. Kraichnan RH (1997) Passive scalar: Scaling exponents and realizability. *Phys Rev Lett* 78(26):4922–4925.
31. Falkovich G, Gawedzki K, Vergassola M (2001) Particles and fields in fluid turbulence. *Rev Mod Phys* 73(4):913–975.
32. Frisch U, Mazzino A, Vergassola M (1998) Intermittency in passive scalar advection. *Phys Rev Lett* 80(25):5532–5535.
33. Gat O, Procaccia I, Zeitak R (1997) Anomalous scaling in passive scalar advection: Monte Carlo Lagrangian trajectories. *Phys Rev Lett* 80(25):5536–5539.
34. Sawford BL, Yeung PK (2015) Direct numerical simulation studies of Lagrangian intermittency in turbulence. *Phys Fluids* 27(6):065109.
35. Yeung PK, Pope SB, Lamorgese AG, Donzis DA (2006) Acceleration and dissipation statistics of numerically simulated isotropic turbulence. *Phys Fluids* 18(6):065103.
36. Schumacher J, et al. (2014) Small-scale universality in fluid turbulence. *Proc Natl Acad Sci USA* 111(30):10961–10965.
37. Sreenivasan KR (1998) An update on the dissipation rate in homogeneous turbulence. *Phys Fluids* 10(2):528–529.